Spectroscopic constraints on UV metal line emission at z 6-9: the nature of Lyα emitting galaxies in the reionization era

Ramesh Mainali, Adi Zitrin, Daniel P. Stark, Richard S. Ellis, Johan Richard, Mengtao Tang, Nicolas Laporte, Pascal Oesch, Ian Mcgreer

Monthly Notices
of the
ROYAL ASTRONOMICAL SOCIETY

MNRAS **479,** 1180–1193 (2018)
Advance Access publication 2018 June 22

doi:10.1093/mnras/sty1640

Spectroscopic constraints on UV metal line emission at $z \simeq 6$–9: the nature of Lyα emitting galaxies in the reionization era

Ramesh Mainali,[1]★ Adi Zitrin,[2] Daniel P. Stark,[1] Richard S. Ellis,[3] Johan Richard,[4] Mengtao Tang,[1] Nicolas Laporte,[3] Pascal Oesch[5] and Ian McGreer[1]

[1]*Steward Observatory, University of Arizona, 933 N Cherry Ave, 85719 Tucson, AZ, USA*
[2]*Physics Department, Ben-Gurion University of the Negev, PO Box 653, Be'er-Sheva, 84105, Israel*
[3]*Department of Physics and Astronomy, University College London, Gower Street, London WC1E 6BT, UK*
[4]*Centre de Recherche Astrophysique de Lyon ,Univ Lyon, Univ Lyon1, Ens de Lyon, CNRS, UMR5574, F-69230 Saint-Genis-Laval, France*
[5]*Geneva Observatory, University of Geneva, Ch. des Maillettes 51, CH-1290 Versoix, Switzerland*

Accepted 2018 June 19. Received 2018 June 13; in original form 2018 March 30

ABSTRACT

Recent studies have revealed intense ultraviolet (UV) metal emission lines in a modest sample of $z > 7$ Lyman-α emitters, indicating a hard ionizing spectrum is present. If such high ionization features are shown to be common, it may indicate that extreme radiation fields play a role in regulating the visibility of Lyα in the reionization era. Here, we present deep near-infrared spectra of seven galaxies with Lyα emission at $5.4 < z < 8.7$ (including a newly confirmed lensed galaxy at $z_{\rm Ly\alpha} = 6.031$) and three bright $z \simeq 7$ photometric targets. In nine sources, we do not detect UV metal lines. However in the $z_{\rm Ly\alpha} = 8.683$ galaxy EGSY8p7, we detect a 4.6σ emission line in the narrow spectral window expected for N vλ1243. The feature is unresolved (FWHM $< 90\,{\rm km\ s^{-1}}$) and is likely nebular in origin. A deep *H*-band spectrum of EGSY8p7 reveals non-detections of C IV, He II, and O III]. The presence of N v requires a substantial flux of photons above 77 eV, pointing to a hard ionizing spectrum powered by an active galactic nucleus or fast radiative shocks. Regardless of its origin, the intense radiation field of EGSY8p7 may aid the transmission of Lyα through what is likely a partially neutral intergalactic medium. With this new detection, five of 13 known Lyα emitters at $z > 7$ have now been shown to have intense UV line emission, suggesting that extreme radiation fields are commonplace among the Lyα population. Future observations with *JWST* will eventually clarify the origin of these features and explain their role in the visibility of Lyα in the reionization era.

Key words: Galaxy: evolution – Galaxy: formation – galaxies: high-redshift – intergalactic medium – quasars: emission lines – dark ages, reionization, first star.

1 INTRODUCTION

The reionization of the intergalactic medium (IGM) is a pivotal milestone in the early universe, marking the point at which almost every baryon has been impacted by structure formation. Over the past two decades, substantial efforts have been devoted to improving our understanding of the process. While our knowledge remains very limited, a picture describing the most basic details of reionization has emerged. Measurement of the optical depth to electron scattering of the cosmic microwave background photons (Planck Collaboration I 2016) and deep spectra of high-redshift quasars (e.g. McGreer, Mesinger & D'Odorico 2015) indicate that the process is underway by $z \simeq 9$ and is completed at or before $z \simeq 6$. Deep imaging surveys with the *Hubble Space Telescope* (*HST*) have enabled the identification of large numbers of colour-selected galaxies over this redshift range (e.g. McLure et al. 2013; Bouwens et al. 2015b; Finkelstein et al. 2015; Atek et al. 2015; Livermore, Finkelstein & Lotz 2017; Ishigaki et al. 2018; for a review see Stark 2016), revealing that faint star-forming galaxies may provide the dominant source of photons required for ionizing intergalactic hydrogen (e.g. Robertson et al. 2015; Bouwens et al. 2015a; Stanway, Eldridge & Becker 2016).

Observational efforts are now focused on mapping the evolution of the IGM at $7 < z < 8$, when the bulk of reionization is thought to occur. Most of what we currently know about the IGM at these redshifts comes from measurements of Lyα emission from star-forming galaxies. As the IGM becomes partially neutral, the damping wing

★ E-mail: rmainali@email.arizona.edu

absorption of intergalactic hydrogen begins to attenuate Lyα emission, reducing the visibility of Lyα emission in star-forming galaxies. The decline of the Lyman-α emitter (LAE) population can be probed by the luminosity function of narrow-band-selected LAEs (e.g. Malhotra & Rhoads 2004; Kashikawa et al. 2006; Ouchi et al. 2010; Hu et al. 2010; Ota et al. 2017; Konno et al. 2018) or the evolution of the Lyα equivalent width (EW) distribution in continuum-selected galaxies (e.g. Stark et al. 2010; Fontana et al. 2010; Ono et al. 2012; Schenker et al. 2014; Pentericci et al. 2014; Tilvi et al. 2014; Caruana et al. 2014; Schmidt et al. 2016). Both tests demonstrate that the visibility of Lyα-emitting galaxies drops significantly in the 170 Myr between $z \simeq 6$ and 7. To explain the magnitude of this drop, it is thought that the IGM must become significantly neutral ($x_{\rm HI} = 0.4$–0.6) by $z \simeq 7$ (e.g. Dijkstra et al. 2014; Mesinger et al. 2015; Mason et al. 2017). While such results were initially met with skepticism, the first handful of quasars at $z > 7$ have suggested similarly large neutral hydrogen fractions (e.g. Mortlock et al. 2011; Greig et al. 2017; Bañados et al. 2018; cf. Bosman & Becker 2015).

Progress in identifying Lyα at $z > 7$ has recently begun to ramp up, revealing a more complex picture than described above. Much of the success has come from a photometric selection of four $z > 7$ galaxies in the CANDELS fields (Roberts-Borsani et al. 2016; hereafter RB16). Each system is very bright ($H \simeq 25$), massive ($\sim 10^{10}$ $M_\odot$ in stars), and red in *Spitzer*/IRAC [3.6]–[4.5] colour, indicating the presence of very strong [O III]+Hβ emission . Follow-up Keck spectroscopy has shown that Lyα emission is present in all four galaxies (Oesch et al. 2015; Zitrin et al. 2015; Stark et al. 2017; RB16), including record-breaking detections at $z = 7.73$ (Oesch et al. 2015) and $z = 8.68$ (Zitrin et al. 2015). The large LAE fraction in the RB16 sample is greater than the success rates found in other galaxy samples at similar redshifts. How Lyα emission can be transmitted so effectively from these four galaxies while being so strongly attenuated from most other systems at $z > 7$ is still not clear.

The conventional explanation is that because of their high mass, the RB16 galaxies trace a clustered population within overdense regions which ionize their surroundings early. As a result, they should be situated in large ionized patches of the IGM, increasing the transmission of Lyα (Mason et al. 2018). The visibility of Lyα in high-mass galaxies is also favoured by the line profile of Lyα that emerges following transfer through the circumgalactic medium. With both a larger linewidth and velocity offset than in lower mass galaxies (Erb et al. 2014; Stark et al. 2017), a larger fraction of Lyα in high-mass galaxies will be redshifted far enough away from line centre to escape the strong damping wing absorption of the neutral IGM (Stark et al. 2017; Mason et al. 2017). Nevertheless surveys for Lyα in other massive star-forming galaxies at $z > 7$ have been met with a much lower success rate than found in the RB16 sample (e.g. Schenker et al. 2014; Bian et al. 2015; Furusawa et al. 2016).

An alternative explanation that is gaining traction posits a link between Lyα visibility at $z > 7$ and the intensity of the galaxy ionizing spectrum. The large [O III]+Hβ emission of both the RB16 galaxies (and several other $z > 7$ LAEs) signals an extreme radiation field that might indicate larger than average Lyα production rates, boosting the likelihood of detection. The connection between Lyα visibility and the hardness of the ionizing spectrum has been strengthened with the discovery of intense ultraviolet (UV) metal line emission (C III], N v, He II) in two of the RB16 galaxies (Stark et al. 2017; Laporte et al. 2017) and two additional colour-selected LAEs at $z > 7$ (Stark et al. 2015b; Tilvi et al. 2016). Such intense high ionization features are extraordinarily rare at lower redshift, likely requiring the presence of an active galactic nucleus (AGN) or metal-poor stellar population (Feltre, Charlot & Gutkin 2016; Gutkin, Charlot & Bruzual 2016; Jaskot & Ravindranath 2016; Nakajima et al. 2017). These results indicate that variations in radiation field may play an important role in regulating Lyα visibility at $z > 7$; failure to account for such variations would lead to an incorrect IGM ionization state.

Here, we present new constraints on the presence of high ionization features in LAEs at $z > 7$, including the first investigation of UV metal lines in the $z = 8.68$ galaxy EGSY8p7. We aim to determine whether extreme radiation fields are present in all LAEs in the reionization era and to better characterize the far-UV spectra of those $z > 7$ systems with existing metal line detections. We detail the spectroscopic observations in Section 2 and describe the spectra of individual sources in Section 3. In Section 4, we discuss implications for the nature of LAEs and review what is known about the distribution of UV metal line EWs at high redshift.

We adopt a Λ-dominated, flat universe with $\Omega_\Lambda = 0.7$, $\Omega_{\rm M} = 0.3$, and $H_0 = 70\,{\rm h_{70}\,km\,s^{-1}\,Mpc^{-1}}$. All magnitudes in this paper are quoted in the AB magnitude system (Oke & Gunn 1983), and all EWs are quoted in the rest frame.

2 OBSERVATIONS

We have obtained near-infrared (NIR) spectroscopic observations of four spectroscopically confirmed Lyα- emitting galaxies at $z > 7$ and an additional three at $5.4 < z < 6.0$. We also have obtained deep spectra of three bright $z \simeq 7$ sources lacking Lyα emission. Observations have been obtained with Keck, Very Large Telescope (VLT), and the Large Binocular Telescope (LBT). Below we describe the observational setup and data reduction procedure.

2.1 Keck/MOSFIRE spectroscopy

The majority of spectra presented in this paper were obtained using the multi-object spectrograph MOSFIRE (McLean et al. 2012) on the Keck I telescope. Over five different observing runs between 2015 and 2017, we targeted $z \simeq 6$–9 galaxies in the EGS, Abell 1703, and Abell 2218 fields . Details of the observations are summarized in Table 1.

The spectra constrain the strength of He II and UV metal emission lines in known $z > 7$ galaxies. Our target selection is driven by the need for sources to have precise redshifts, bright continuum flux, and redshifts which place at least one of the strong UV lines at a wavelength with significant atmospheric transmission. We designed five separate masks which are described in more detail below. For each mask, we included 1 or 2 isolated stars to monitor seeing and to calculate the absolute flux calibration. Each mask is constructed with slit widths of 0.7 arcsec. Below we briefly describe the observing conditions and key targets. More details on the physical properties of the sources will be provided in Section 3.

The EGS CANDELS area contains three of the 13 $z > 7$ galaxies with S/N>5 Lyα detections. We designed two masks to cover the three targets. The first mask was focused on EGSY8p7, the $z = 8.68$ galaxy confirmed in Zitrin et al. (2015). At this redshift, we are able to probe C IV, He II, and O III] in the H band. The C III] line is situated between the H and K bands in a region of poor atmospheric transmission. We obtained 5.93 h of on-source integration in H band on the mask on 2016 April 29–30. Conditions were clear with seeing of 0.8 arcsec. The mask was filled with lower redshift ($z \simeq 1$–2) sources picked to have extreme EW rest-frame optical emission lines in the H band. We will discuss the spectra of the filler sources in a separate paper (Tang et al., in preparation).

Table 1. Galaxies targeted in this study. A383−2211 was observed with the VLT/X-shooter, J14144+5446 with the LBT/LUCI, and the rest were observed with the Keck/MOSFIRE. The final column provides the reference to the article where the objects were originally identified. References: [1] Roberts-Borsani et al. (2016); [2] Zitrin et al. (2015); [3] Oesch et al. (2015); [4] Stark et al. (2017); [5] Schenker et al. (2012); [6] Stark et al. (2015b); [7] Bradley et al. (2014); [8] Ellis et al. (2001) ; [9] McGreer et al. (2018) ; [10] Bradley et al. (2012); and [11] Kneib et al. (2004).

Source	Redshift	RA	Dec.	Date of observations	Filters	t_{exp} (h)	UV lines targeted	Ref
				Spectroscopic targets				
EGSY8p7	8.683	14:20:08.50	+52:53:26.6	2016 Apr 29–30	H	5.93	C IV, He II, O III]	[1],[2]
EGS-zs8-1	7.730	14:20:34.89	+53:00:15.4	2016 May 2–3	J	4.53	C IV	[1], [3],[4]
...	...	...	...	2017 Jul 31	J	1.87	C IV	[1], [3], [4]
EGS-zs8-2	7.477	14:20:12.09	+53:00:27.0	2016 May 2–3	J	4.53	C IV	[1], [4]
...	...	...	...	2017 Jul 31	J	1.87	C IV	[1], [4]
A1703-zd6	7.045	13:15:01.01	+51:50:04.3	2016 Apr 29	H	2.47	C III]	[5],[6]
A383-2211	6.031	02:48:01.39	−03:32:58.4	2013 Dec 15,18,and 25	VIS	4.78	Lyα	[7]
...	...	...	...	...	NIR	...	C IV, He II, O III], C III]	[7]
Abell2218-S3.a	5.576	16:35:51.96	+66:12:45.9	2015 Sep 08	J	1.33	C III]	[8]
...	...	...	...	2016 Apr 29	J	1.20	C III]	[8]
Abell2218-S3.b	5.576	16:35:52.08	+66:12:51.8	2015 Sep 08	J	1.33	C III]	[8]
...	...	...	...	2016 Apr 29	J	1.20	C III]	[8]
J14144+5446	5.426	14:14:46.82	+54:46:31.9	2015 Apr 07	J	1.08	C III]	[9]
				Photometric targets				
A1703-zD4	$8.4^{+0.9}_{-1.4}$	13:15:07.19	51:50:23.5	2016 Apr 29	H	2.47	C III]	[10]
A1703-zD1	$6.7^{+0.2}_{-0.1}$	13:14:59.42	51:50:00.8	2016 Apr 29	H	2.47	C III]	[10]
Abell2218-C1.b	$6.7^{+0.1}_{-0.1}$	16:35:54.40	66:12:32.8	2016 Apr 29	J	1.20	C IV, He II, O III]	[11]
Abell2218-C1.c	$6.7^{+0.1}_{-0.1}$	16:35:48.92	66:12:02.4	2016 Apr 29	J	1.20	C IV, He II, O III]	[11]

The other two $z > 7$ LAEs in the EGS field, EGS-zs8-1 ($z = 7.73$) and EGS-zs8-2 ($z = 7.47$), are close enough to fit on the same MOSFIRE mask. We previously obtained MOSFIRE *H*-band observations of both systems, revealing strong C III] emission in EGS-zs8-1 and no C III] emission in EGS-zs8-2 (Stark et al. 2017). Here, we present new *J*-band observations aimed at constraining the strength of C IV emission in both galaxies. The O III] and *He* II emission lines are situated between the *J* and *H* bands where atmospheric transmission is low. As with our other EGS mask, we included $z \simeq 1$–2 extreme emission-line galaxies as filler targets. We obtained a total of 6.4 h of integration in *J* band, with 4.53 h secured over 2016 May 2–3 and an additional 1.87 h on 2017 July 31. Conditions were clear for both runs with seeing of 0.7arcsec (2016 May) and 0.9 arcsec (2017 July).

The Abell 1703 field has several bright gravitationally lensed $z \gtrsim 7$ galaxies that are ideal for spectroscopic study (Bradley et al. 2012), including an LAE at $z_{Ly\alpha} = 7.045$ (A1703-zd6; Schenker et al. 2012) and six additional targets with photometric redshifts between $z \simeq 6.4$ and 8.8. We previously targeted the field in *J* band, revealing nebular C IV emission in A1703-zd6 (Stark et al. 2015b). We now target C III] emission in A1703-zd6 with *H*-band observations of the Abell 1703 field. We also include the photometric $z \gtrsim 7$ targets A1703-zd1 and A1703-zd4 on the mask, with the goal of constraining C III] in the former and C IV, He II, O III], and C III] in the latter. Empty real estate on the mask was filled with targets detected with *Herschel* (Walth et al., in preparation). Conditions were clear with seeing of 0.7 arcsec throughout the 2.47 h of on-source integration time on 2016 April 29.

The Abell 2218 cluster field has two relevant sources for UV metal line follow-up: A2218−S3, a multiply imaged LAEs at $z_{Ly\alpha} = 5.576$ (Ellis et al. 2001) and A2218−C1, a bright triply imaged $z \simeq 6.7$ galaxy lacking Lyα emission (Kneib et al. 2004; Egami et al. 2005). We designed a mask that includes the two images of the $z_{Ly\alpha} = 5.576$ galaxy (S3a, S3b) and two of the images of the $z \simeq 6.7$ source (C1b, C1c). We filled the mask with other lensed galaxies in the field: C2.a ($z \simeq 3.104$; Richard et al. 2011a), C3.a ($z \simeq 2.8$; Elíasdóttir et al. 2007), S2.1.a ($z = 2.51$; Ebbels et al. 1996), and S6.a ($z = 1.03$; Kneib et al. 1996). We observed the mask for a total of 1.2 h in the *J* band on 2016 April 29. For the $z_{Ly\alpha} = 5.576$ galaxy, we also added data from a previous program (PI: Zitrin) who observed the galaxy for 1.33 h on 2015 September 08. Both nights were clear with seeing of 0.9 arcsec (2015 September) and 0.8 arcsec (2016 April).

Data were reduced using the publicly available MOSFIRE Data Reduction Pipeline. The pipeline performs flat fielding, wavelength calibration, and background subtraction. The reduction process outputs 2D reduced spectra along with a signal-to-noise (S/N) map and error map for each slit on the mask. Finally, 1D spectra were obtained using a boxcar extraction with an aperture size of 1.5× observed seeing, typically 6–8 pixels (1.08–1.44 arcsec). The flux calibration was performed in two stages. The telluric correction was first applied using long-slit observations of a spectrophotometric standard star that we targeted prior to the science observations. The absolute flux calibration was then calculated using the known fluxes and observed counts of the isolated stars on the mask. The spectral resolution is calculated by fitting the width of isolated sky lines. For our chosen slit widths, we derive an average full width at half-maximum (FWHM) of 3.8 Å in the *J* band and 4.7 Å in the *H* band.

2.2 VLT/X-Shooter spectroscopy

One additional source (A383 − 2211) was observed as a part of programme 092.A-0630(A) (PI: Richard) with the instrument X-Shooter (Vernet et al. 2011) on the VLT. The observations were performed on the nights of 2013 December 15, 18, and 25 for six observing blocks (OBs) of 1 h each. Each OB comprised three exposure of 955 s in the visible (VIS) arm and three exposures of 968

seconds in the NIR arm. The VIS arm provided wavelength coverage from 5336 to 10 200 Å at a spectral resolution of 1.1 Å, whereas the NIR arm provides coverage from 9940 to 24 750 Å at a spectral resolution of 2.1 Å. We used a slit of 11.0 arcsec × 0.9 arcsec size oriented at a position angle of 90°. The observations were conducted using a dither sequence of ±2.5 arcsec along the slit. The conditions were clear with an average seeing of 0.6 arcsec.

The data reduction was performed using version 2.2.0 of the X-Shooter pipeline. The details of the procedure were presented in Stark et al. (2015a). The pipeline outputs 18 reduced exposures which we then combine using standard IDL and IRAF routines. A spectroscopic standard star was observed on the same night to calibrate flux of the spectrum. Multiple telluric stars were observed to calculate a median telluric correction for telluric absorption in the NIR arm.

2.3 LBT/LUCI spectrosocopy

We observed the $z_{Ly\alpha} = 5.426$ LAE J141446.82+544631.9 (hereafter J1414+5446; McGreer et al. 2018) on 2015 April 07 for 1.08 h using the LUCI near-IR spectrograph on the LBT. We used the N1.8 camera and 210_zJHK grating in long-slit mode. The observations were conducted in the *J* band with the goal of constraining the strength of the C III] emission line. A slit width of 1.0 arcsec was used, resulting in a spectral resolution of 2.93 Å. A bright reference star (*J*=17.9) was placed along the slit to monitor seeing and calibrate the absolute flux scale. Data were taken with a standard ABBA dither sequence with a 7.0 arcsec offset between the A and B positions. Conditions were clear with seeing of 1.0 arcsec throughout the observations.

The reduction was performed using an IDL long-slit reduction package for LUCI (see Bian et al. 2010 for details). The package provides flat fielding and sky subtraction using standard routines. The wavelength solution was calculated using night sky lines. The software outputs a fully reduced 2D spectrum which we visually examined for faint emission lines. We identified the spatial position of the galaxy on the spectrum using the trace of the reference star and the known angular offset between the star and galaxy. A 1D spectrum was created using a boxcar extraction with a 6 pixel (1.5 arcsec) aperture. The extracted spectrum was corrected for telluric absorption using the A0V star spectrum, and the absolute flux scale of the extracted spectrum was then derived using the flux of the reference star on the slit.

3 RESULTS

We describe new UV spectral line constraints for the targets presented in Section 2. For each source, we first summarize known physical properties and then detail the results of the newly obtained spectra.

3.1 EGSY8p7

EGSY8p7 is a bright ($H_{160} = 25.3$) galaxy identified by RB16 and confirmed spectroscopically by Zitrin et al. (2015) via detection of Lyα emission at $z_{Ly\alpha} = 8.683$ in a *J*-band spectrum obtained with MOSFIRE (see Fig. 1). The red IRAC colour ([3.6]−[4.5]=0.76) is consistent with the presence of strong [O III]+Hβ emission in the [4.5] filter. A combined [O III]+Hβ rest-frame EW of 895 ± 112 Å is required to explain the [4.5] flux excess relative to the underlying continuum (Stark et al. 2017).

The *J*-band spectrum and the new *H*-band spectrum cover 11530 to 13458 Å and 14587 to 17914 Å, respectively, corresponding to 1191 to 1390 Å and 1506 to 1850 Å in the rest frame. In addition to Lyα, this wavelength range allows constraints to be placed on N V, C IV, He II, and O III]. We guide our search of these lines using the Lyα redshift and the characteristic velocity offset of Lyα from systemic. We consider Lyα velocity offsets between 0 and 500 km s^{-1} (Erb et al. 2014; Stark et al. 2017), implying systemic redshifts in the range $z_{sys} = 8.667$–8.683 for EGSY8p7. Nebular He II, and O III] are typically found to trace the systemic redshift (e.g. Shapley et al. 2003; Stark et al. 2014; Senchyna et al. 2017), so we predict a spectral window for each line using the range of systemic redshifts derived above. C IV is a resonant transition and is found at redshifts between systemic and that of Lyα (Christensen et al. 2012; Stark et al. 2014, 2015b; Vanzella et al. 2016, 2017; Mainali et al. 2017; Laporte et al. 2017; Berg et al. 2018), so we consider a spectral window ranging from the lowest possible systemic redshift ($z_{sys} = 8.667$) and the Lyα redshift ($z_{Ly\alpha} = 8.683$).

We first consider constraints on C IV, He II, and O III] from the new *H*-band spectrum. Taking the range of possible systemic redshifts for EGSY8p7 that we derive above, we predict spectral windows for C IVλ1548 (14966–14991 Å), C IVλ1550 (14991–15016 Å), He IIλ1640 (15860–15885 Å), O III]λ1661 (16055–16082 Å), and O III]λ1666 (16106–16133 Å). As can be seen in Fig. 2, each window is mostly (>80 per cent) free from strong skylines. No significantly detected emission lines are seen. We calculate typical 3σ line flux limits in each spectral window by summing the error spectrum in quadrature over 10 Å (∼200 km s^{-1}). As this is at the upper bound of linewidths found for UV nebular emission lines other than Lyα at these redshifts (e.g. Stark et al. 2014; Bayliss et al. 2014; James et al. 2014; Mainali et al. 2017), it provides a conservative estimate of our sensitivity to emission lines. To calculate the limits on the EW, we compute the continuum flux density expected at the wavelength of each spectral line using the broad-band SED fit in our previous studies (e.g. Zitrin et al. 2015; Stark et al. 2017). The measured limits on line flux and EW are presented in Table 2. The non-detections place strong constraints on C IV and O III], implying that the individual components of each doublet likely have rest-frame EWs below 4.6 Å. Because He II is located in a somewhat noisier region, our constraints are less stringent. The non-detection implies a rest-frame EW below 14.8 Å provided the He II feature is not obscured by the single skyline in the predicted spectral window (see Fig. 2).

We now consider constraints on nebular N V in the *J*-band discovery spectrum from Zitrin et al. (2015). For redshifts between $z_{sys} = 8.667$ and 8.683, we expect N Vλ1238 and N Vλ1243 to lie between 11975 and 11995 Å, and 12017 and 12037 Å, respectively. An emission feature (S/N = 4.6) is seen centred at 12019.5 Å (Fig. 1), within the window where N Vλ1243 would be expected. The feature is at the exact spatial position of the Lyα line and is adjacent to but cleanly separated from skylines. The line is unresolved in the MOSFIRE spectrum (FWHM<90 km s^{-1}). We find that an aperture of 6 pixels (∼2× the spectral resolution) maximizes the S/N. We directly integrate the object and error spectrum (the latter in the quadrature) over this window, revealing a line flux of 2.8 × 10^{-18} erg s^{-1} cm^{-2} and an error (1σ) of 0.6 × 10^{-18} erg s^{-1} cm^{-2}. If the line is N Vλ1243, the blue component of the doublet would be situated near two strong skylines (Fig. 1) making detection difficult. Nevertheless, we do detect positive emission at the precise wavelength predicted for the N Vλ1238 feature (11981 Å), but the skylines prohibit accurate flux measurement.

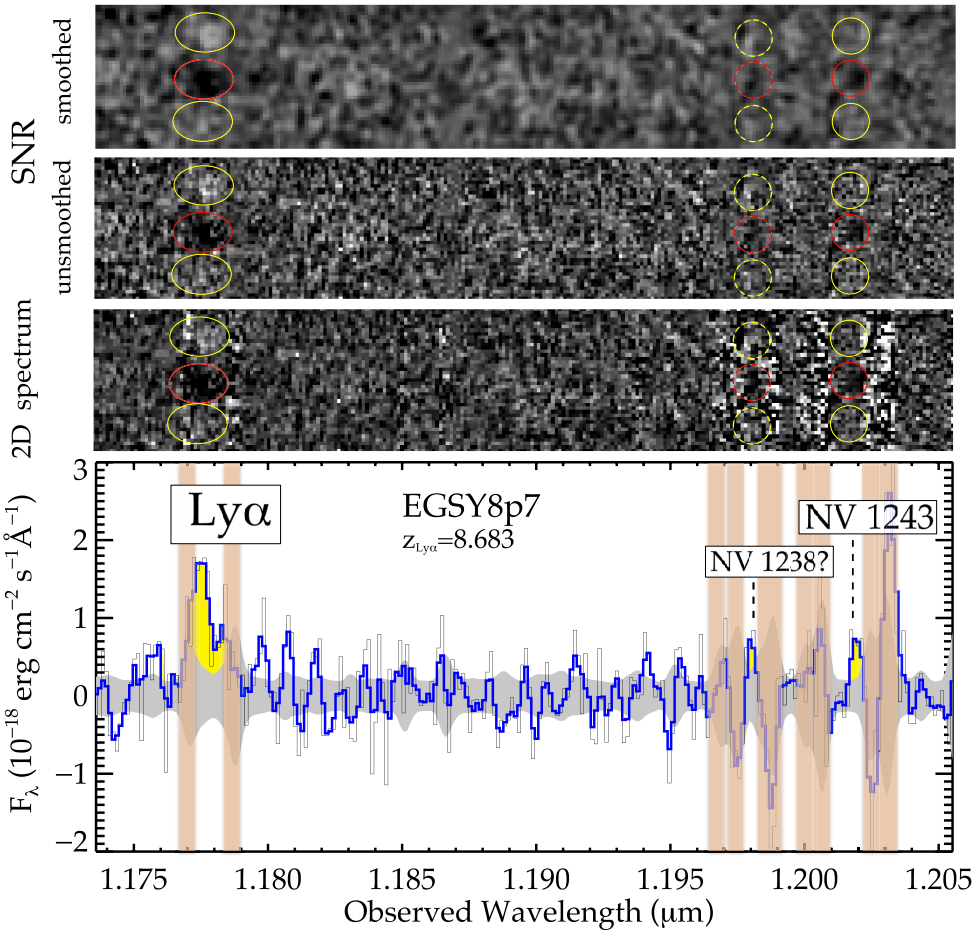

Figure 1. Keck/MOSFIRE 2D and 1D *J*-band spectrum of EGSY8p7 similar to that originally published in Zitrin et al. (2015). Top: the 2D S/N map (smoothed and unsmoothed) showing the N vλ1243 detection where positive fluxes are denoted by black. The red circle shows positive peak of the detection at the same spatial position as expected from Lyα emission, while yellow circles denote negative peaks as expected per the dither sequence. The red dotted circle denote the tentative positive flux from the N vλ1238 component, while yellow dotted circles denote the location of negative peaks as per dither sequence. Middle: similar figure as the top panel showing the 2D spectrum. Bottom: 1D spectrum showing the Lyα line along with the N vλ1243 and tentative N vλ1238 emission features. The black curve denotes the extracted 1D flux whereas the grey region indicates 1σ noise level. The smoothed (2-pixel) flux is shown in blue curve.

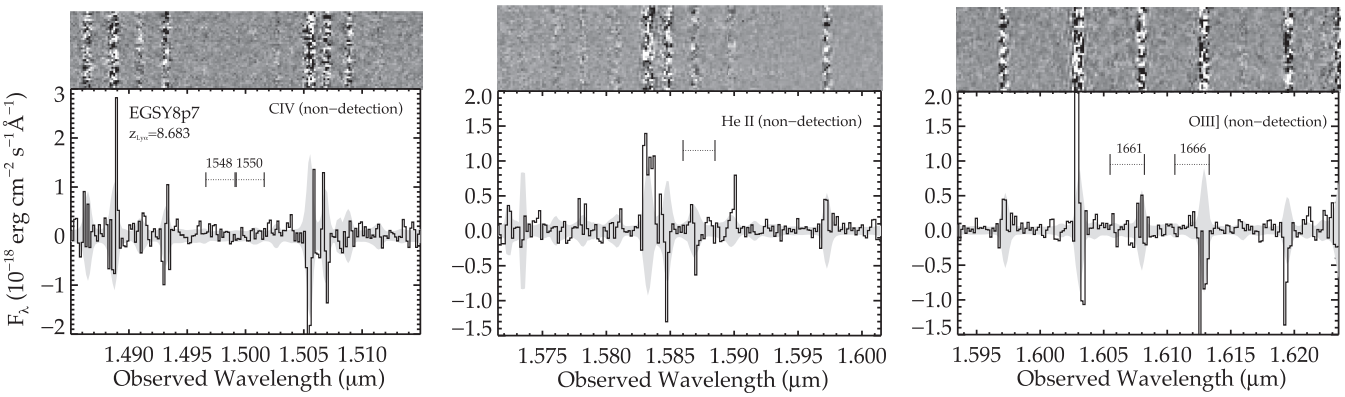

Figure 2. MOSFIRE 2D spectrum (top) and 1D spectrum (bottom) of EGSY8p7 showing the spectral region around expected location of C IV (left), He II (middle), and O III] (right). The black curve denotes the extracted 1D flux, whereas the grey region indicates 1σ noise level. The dotted black lines represent the spectral window where we expect the relevant lines to fall. See Section 3.1 for details.

The odds of finding a 4.6σ feature at the spatial position of Lyα and within the narrow 500 km s^{-1} (16 pixel) spectral window defined above are exceedingly low. We can test this by generating a large number (10^6) of realizations of the error spectrum in the 16 pixel box surrounding the putative N vλ1243 detection. We find features with S/N in excess of 4.6 in only 32 of the 10^6 realizations, implying a very low probability (0.003 per cent) that the line is not real (Fig. 3). We further investigate the likelihood of the detection

Table 2. Rest-UV emission-line constraints on sources presented in this paper. The EWs are given in rest frame. The limits on line fluxes and EWs are quoted as 3σ.

Object	$z_{Ly\alpha}$	Line	λ_{rest} (Å)	Line flux (10^{-18} erg cm^{-2} s^{-1})	EW (W_0) (Å)	Absolute magnitude (M_{UV}) (AB)
			Spectroscopic targets			
EGSY8p7	8.683	N v	1242.80	2.8 ± 0.6	4.2 ± 0.9	$-21.9^{+0.1}_{-0.1}$
	...	C iv	1548.19	<1.6	<4.6	...
	...	...	1550.77	<1.6	<4.6	...
	...	He ii	1640.52	<5.3	<14.8	...
	...	O iii]	1660.81	<1.5	<4.6	...
	...	...	1666.15	<1.5	<4.6	...
EGS-zs8-1	7.730	N v	1238.82	<6.0	<7.4	$-22.1^{+0.1}_{-0.1}$
	...	N v	1242.80	<24.3	<29.6	...
	...	C iv	1548.19	<11.0	<17	...
EGS-zs8-2	7.477	N v	1238.82	<1.7	<2.2	$-21.9^{+0.1}_{-0.1}$
	...	N v	1242.80	<3.6	<4.5	...
	...	C iv	1548.19	<1.2	<2.4	...
	...	...	1550.77	<1.2	<2.4	...
A1703-zd6	7.045	[C iii]	1906.68	<3.3	<19.8	$-19.3^{+0.1}_{-0.4}$
	...	C iii]	1908.73	<3.3	<19.8	...
A383 − 2211	6.031	Lyα	1215.67	16.4 ± 1.4	21.1 ± 2.8	$-20.9^{+0.2}_{-0.2}$
	...	N v	1238.82	<3.8	<4.9	...
	...	N v	1242.80	<3.8	<4.9	...
	...	C iv	1548.19	<2.5	<4.6	...
	...	...	1550.77	<1.3	<2.3	...
	...	He ii	1640.52	<5.3	<12.2	...
	...	O iii]	1660.81	<2.5	<5.7	...
	...	...	1666.15	<4.9	<11.2	...
	...	[C iii]	1906.68	<1.7	<5.8	...
	...	C iii]	1908.73	<1.2	<4.1	...
Abell 2218_S3	5.576	[C iii]	1906.68	<3.2	<15.6	$-16.9^{+0.4}_{-0.3}$
	...	C iii]	1908.73	<3.2	<15.6	...
J14144+5446	5.426	[C iii]	1906.68	<12.0	<7.3	$-21.1^{+1.6}_{-0.1}$
	...	C iii]	1908.73	< 8.4	<5.2	...
			Photometric Targets			
A1703-zd4	$8.4^{+0.9}_{-1.4}$	C iv, He ii, O iii],C iii]	...	< 5.7	<20	$-20.6^{+0.2}_{-0.5}$
A1703-zD1	$6.7^{+0.2}_{-0.1}$	C iii]	...	< 5.3	<6.8	$-20.5^{+0.2}_{-0.8}$
Abell 2218−C1	$6.7^{+0.1}_{-0.1}$	C iv, He ii, O iii]	...	< 7.1	<5.5	$-19.4^{+0.2}_{-0.3}$

by looking at the significance of the emission in subsets of the stacked spectrum. The *J*-band data were obtained over two nights (see Zitrin et al. 2015 for details) with integration times of 158 min (night one) and 128 min (night two) contributing to the total stack. The data from the first night were obtained under significantly better conditions (seeing of 0.6 arcsec) than the second night (0.8 arcsec). As reported in Zitrin et al. (2015), the Lyα detection significance is higher in the night one stack (S/N=6.0) than in the night two data (S/N=3.8), consistent with expectations given the longer integration time and improved seeing. The significance of the N vλ1243 feature is also found to be larger on night 1 (S/N=4.1) relative to night 2 (S/N=2.0). The increase in significance between night two and night one is consistent with that measured for Lyα. The fact that the significance of the feature scales with atmospheric conditions in a manner consistent with Lyα further bolsters confidence that the N v detection is real and associated with EGSY8p7.

The rest-frame EW implied by the N vλ1243 detection is 4.2 ± 0.9 Å. Here, we derive the continuum flux (and associated error) from the broad-band SED, as is standard at these redshifts. We include the error in the underlying continuum and line flux in the EW, and we take care to not include filters contaminated by nebular emission in our derivation of the continuum flux. The uncertainty in the EW is dominated by the line flux uncertainty which is 22 per cent. Using the standard theoretical flux ratio for the N v doublet (N vλ1238/N vλ1243=2, Bickel 1969; Torres-Peimbert & Pena 1984), we can estimate the total flux ($8.4 \pm 1.8 \times 10^{-18}$ erg cm^{-2} s^{-1}) and rest-frame EW (12.6 ± 1.8 Å). The observed wavelength of the likely N vλ1243 feature would indicate a redshift of $z = 8.671$, implying a Lyα velocity offset (from Nv) of 362 km s^{-1}. While N v is a resonant transition, it has been shown to trace the systemic redshift to within 20 km s^{-1} in another of the $z > 7$ LAEs (Pentericci et al. 2016; Laporte et al. 2017). If the likely N v feature also traces the systemic redshift in EGSY8p7, it would indicate a large Lyα velocity offset, consistent with other similarly massive sources at high redshift (e.g. Erb et al. 2014; Stark et al. 2017). Such a large velocity offset may aid in the escape of Lyα through the IGM (Mason et al. 2017).

3.2 EGS-zs8-1 and EGS-zs8-2

Our second mask in the EGS contained EGS-zs8-1 and EGS-zs8-2 from RB16. Both are bright ($H_{160} = 25.0$ and 25.1, respectively) and have red IRAC [3.6]−[4.5] colours that suggest strong [O iii]+Hβ emission (EW = 911 ± 122 and 1610 ± 302 Å rest frame, respectively (Stark et al. 2017). Detections of Lyα in EGS-zs8-1 and EGS-zs8-2 confirm their redshifts to be $z_{Ly\alpha}$=7.730 (Oesch et al.

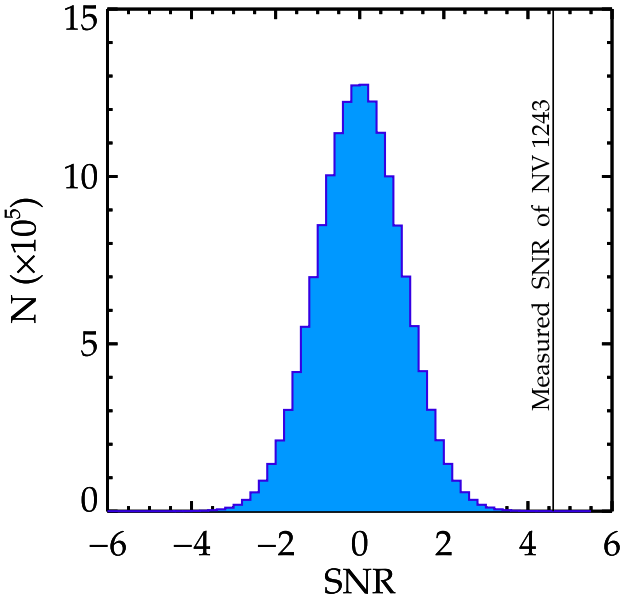

Figure 3. The S/N distribution in 10^6 realizations of the error spectrum within the 16 pixel window defined by the Lyα (see Section 3.1). Apertures of size 6 × 6 pixel, similar to the one used to measure the N v detection, were used to estimate the S/N. The vertical black line denotes the detected significance of the N v 1243 line.

2015) and 7.477 (RB16, Stark et al. 2017). *H*-band MOSFIRE observations presented in Stark et al. (2017) revealed C III] emission in EGS-zs8-1 (rest-frame EW of 22 ± 2 Å) and a non-detection in EGS-zs8-2. The latter provides a 3σ upper limit on the total C III] EW in EGS-zs8-2 of 14.2 Å. Our new *J*-band spectra allow us to constrain the strength of C IV emission in both sources. As with EGSY8p7, we predict the wavelength of C IV using estimates of the systemic redshift. The systemic redshift of EGS-zs8-1 ($z_{\rm sys}$ = 7.723) is determined using the wavelength of the [C III], C III] doublet. For EGS-zs8-2, we consider systemic redshifts in the range $z_{\rm sys}$ = 7.463–7.477, following the same approach as we took for EGSY8p7.

We consider N v redshifts between that of systemic and Lyα. For EGS-zs8-1, this implies a spectral window of 10797–10815 Å (N vλ1238 and 1243). These wavelengths are covered in the discovery *Y*-band MOSFIRE spectrum presented in Oesch et al. (2015). The N vλ1238 window is completely clear of skylines, while 37 per cent of the N vλ1243 window is obscured. No emission lines are detected in either window, implying 3σ upper limits on the EW of N vλ1238 (<7.4 Å) and N vλ1243 (<29.6 Å). As N vλ1238 is the stronger of the two components, its absence in the *Y*-band spectrum confirms that N v is not present in EGS-zs8-1 at the same intensity as it is found in EGSY8p7. The redshift of EGS-zs8-1 makes detection of C IV difficult. The *J*-band spectrum covers 11530–13520 Å, corresponding to rest-frame wavelengths between 1320 and 1549 Å. This places C IVλ1548 at the red edge of the *J* band where sensitivity is reduced and cuts out the λ1550 component entirely. To predict the observed wavelength of C IVλ1548, we again consider C IV redshifts between that of systemic and Lyα. This translates into a spectral window spanning 13493–13515 Å. No emission line is visible. For a 10 Å linewidth, we derive a 3σ limiting flux (rest-frame EW) of 1.1 × 10^{-17} erg cm^{-2} s^{-1} (17 Å) for C IVλ1548. We can use the theoretical line ratio of C IV doublet components (C IVλ1548/C IVλ1550=2) to derive an upper limit on the total C IV doublet strength (1.7 × 10^{-17} erg cm^{-2} s^{-1}), implying a rest-frame EW below 29 Å. The C IV non-detection places a 3σ upper bound on the C IV/C III] flux ratio in EGS-zs8-1 of less than 2.1. This is consistent with expectations for nebular lines powered by massive stars and AGN (e.g. Feltre et al. 2016; Jaskot & Ravindranath 2016; Byler et al. 2018). The lack of atmospheric absorption will enable *JWST* to extend these UV line measurements to deeper limits.

The *J*-band spectrum of EGS-zs8-2 (Fig. 4a) probes rest-frame wavelengths between 1360 and 1596 Å, allowing constraints to be placed on the strength of nebular C IV. The absence of strong C III] in EGS-zs8-2 could potentially reflect a hard ionizing spectrum that produces a large C IV/C III] ratio. Following the same approach as above, we consider a window between 13102 and 13124 Å for C IVλ1548 and 13124 and 13146 Å for C IVλ1550. The C IVλ1548 window is free of strong skylines, but no convincing nebular emission is apparent. The non-detection of C IVλ1548 in this window allows us to place a 3σ upper limit of 1.2 × 10^{-18} erg cm^{-2} s^{-1} and 2.4 Å for the line flux and rest-frame EW, respectively. There is a skyline that covers 21 per cent of the C IVλ1550 spectral window. While the red component of the doublet could be obscured by this sky feature, the blue component (stronger by a factor of two) would have been visible if C IV emission was strong. The non-detection of the doublet suggests that the total EW of nebular C IV is below 4.8 Å (3σ) for EGS-zs8-2. We also consider the presence of N v in the *Y*-band Keck/MOSFIRE spectrum presented in Stark et al. (2017). No emission lines are seen in the predicted windows for N vλ1238 (10484–10501 Å) and N vλ1243 (10518 –10535 Å). As both of these wavelength ranges are mostly free of strong skylines, the non-detection provides a 3σ upper limit to the rest-frame EW of N vλ1238 (<2.2 Å) and N vλ1243 (<4.5 Å). EGS-zs8-2 is thus the only of the four RB16 sources lacking a UV metal line detection, likely implying a less extreme radiation field.

3.3 Abell 1703

The top priority target on our Abell 1703 mask was A1703-zd6, a bright gravitationally lensed galaxy (H_{160} = 25.9) first identified by Bradley et al. (2012). Lyman-α emission was detected at 9780 Å, indicating a redshift of $z_{{\rm Ly}\alpha}$ = 7.045 (Schenker et al. 2012). After correcting for cluster magnification (μ = 5.2), the absolute magnitude of A1703-zd6 is relatively faint ($M_{\rm UV}$ = −19.3), providing a glimpse of the properties of a lower mass reionization-era system with visible Lyα emission. A *J*-band spectrum obtained with MOSFIRE revealed strong C IVλλ1548,1550 emission (EW = 38 Å rest frame, Stark et al. 2015b), requiring a hard ionizing spectrum with 48 eV photons capable of triply ionizing carbon. Since C IV is a resonant line, we cannot use it to determine the systemic redshift. Using the same approach as for the EGS targets, we predict that the systemic redshift should be in a window spanning from $z_{\rm sys}$ = 7.032 to 7.045.

The new *H*-band spectrum of A1703-zd6 (Fig. 4b) probes 14560–17880 Å, corresponding to 1813–2214 Å in the rest frame, allowing constraints to be placed on the strength of C III] emission. By constraining the line ratio of C IV/C III], we hope to better constrain the shape of the ionizing spectrum powering the intense nebular emission. The range of possible systemic redshifts situates [C III]λ1907 at 15313–15339 Å and C III]λ1909 at 15330–15356 Å. We detect no emission line in either window. While there is a skyline that covers 18 per cent of each window, there is no configuration where both the λ1907 and λ1909 components are obscured. If one line

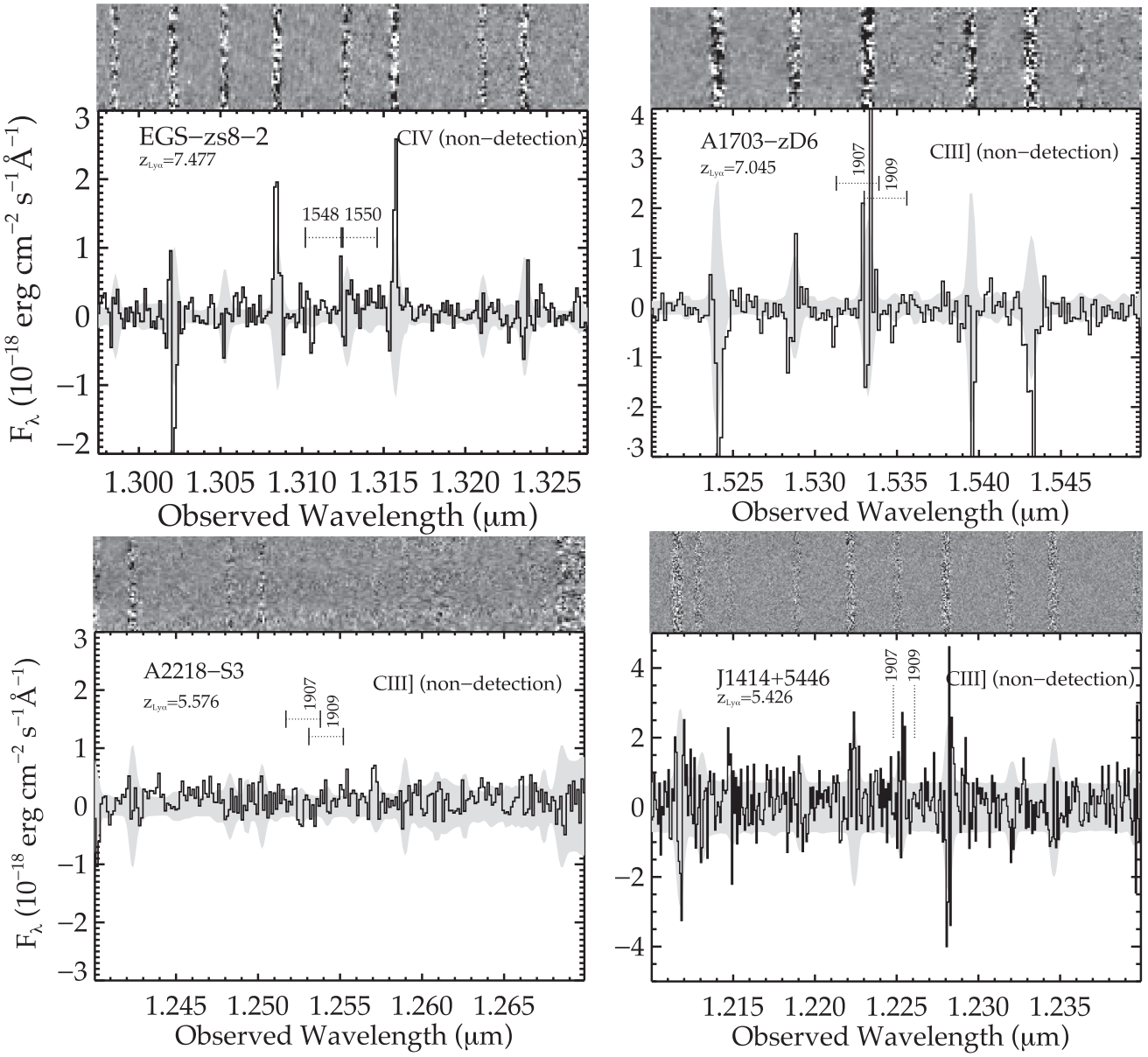

Figure 4. 2D spectrum and 1D spectrum of EGS-zs8-2 (upper left), A1703_zD6 (upper right), Abell2218−S3 (bottom left), and SDSS J1414+5446 (bottom right) . The black curve denotes the extracted 1D flux density, whereas the grey region indicates 1σ noise level. The dotted black lines represent the spectral window where we expect the relevant lines to fall.

is obscured, then the other component should be in a clean part of the spectrum. We calculate a 3σ limiting flux (EW) of 3.3 × 10^{-18} erg cm^{-2} s^{-1} (19.8 Å) for each component of the C III]λλ1907,1909 doublet, where we have again assumed a 10 Å FWHM for the line. The absence of C III] suggests that A1703-zd6 has a C IV/C III] line ratio of >1.2 (3σ), consistent with the C IV/C III] flux ratios (1.3–6.6) seen in AGN at lower redshifts (e.g. Dors et al. 2014; Feltre et al. 2016). Metal-poor galaxies with nebular C IV emission have also been observed with C IV/C III] ratios in excess of 1.0 (e.g. Vanzella et al. 2016, 2017; Mainali et al. 2017), so the current limits do not rule out massive stars as a powering mechanism. Deep constraints on He II and N V provide the best path toward determining the origin of the C IV emission.

The MOSFIRE mask in Abell 1703 also allows us to place constraints on UV emission lines in two $z \gtrsim 6$ targets that lack spectroscopic redshifts. A1703-zd1 is one of the brightest ($H = 24.0$) galaxies at $z \simeq 7$. Using broad-band photometry from *HST*, Bradley et al. (2012) derived a photometric redshift of $z = 6.7^{+0.2}_{-0.1}$. The galaxy is highly magnified ($\mu = 9.0$) implying an absolute UV magnitude of $M_{UV} = -20.5$. Deep z- and J-band spectra have failed to reveal any emission lines in A1703-zd1, providing upper limits on the flux of Lyα (Schenker et al. 2012) and C IV, He II, and O III] (Stark et al. 2015b). By obtaining an H-band spectrum which covers 14500–17800 Å, we now constrain the strength of C III] emission. The range of possible photometric redshifts places [C III]λ1907 between 14493 and 15065 Å and C III]λ1909 between 14508 and 15081 Å. The region is largely free of OH lines, with 59 per cent of the wavelength range having a 5σ flux limit of 5.3 × 10^{-18} erg cm^{-2} s^{-1}. This corresponds to a rest-frame EW of 6.8 Å for individual components of the [C III], C III] doublet after an aperture correction

of 1.09× is applied to the line flux to account for the slit losses from this extended arc.

We apply a similar analysis to A1703-zd4, another bright ($H_{160} = 25.4$) galaxy with a photometric redshift of $z = 8.4$. The photometry allows a broader range of redshifts for this target, with acceptable solutions between $z = 7.0$ and 9.3 (Bradley et al. 2012). The source is magnified by $\mu = 3.1$ implying an absolute UV magnitude of $M_{\rm UV} = -20.6$. The *J*-band spectrum from Stark et al. (2015b) constrains Lyα over $8.5 < z < 10.1$ and C IV over $6.4 < z < 7.7$. The absence of emission lines in the *J* band suggests a 5σ EW limit of 6 Å for Lyα and C IV lines situated between OH emission lines. The newly acquired *H*-band spectrum samples wavelengths between 14810 and 18140 Å, and is sensitive to C IV at redshifts $8.57 < z < 10.69$, He II at $8.03 < z < 10.05$, O III] at $7.89 < z < 9.92$, and C III] at $6.76 < z < 8.34$. No emission is visible throughout the spectrum. For regions between sky lines (60 per cent of the spectrum), we measure a 5σ flux limit of 5.7×10^{-18} erg cm^{-2} s^{-1}. This implies a rest-frame EW limit of 20 Å for lines located in clean regions of the *J*-band spectrum.

3.4 Abell 2218

A2218−S3 is a multiply imaged LAE at $z_{\rm Ly\alpha} = 5.576$ (Ellis et al. 2001). Both images (A2218−S3a and S3b) show Lyα emission with an estimated rest-frame EW of 239 ± 25 Å. The galaxy is fainter than the others reported in this paper ($H_{160} = 26.6$ and 26.7 for images a and b, respectively; Richard et al. 2007). After correcting for the magnification of a and b ($\mu = 33.1$ and 30.2), the absolute UV magnitude is found to be the faintest in our sample ($M_{\rm UV} = -16.9$). The MOSFIRE *J*-band spectra of A2218−S3a and A2218−S3b cover 11530–13520 Å, corresponding roughly to 1753 and 2055 Å for both targets. For Lyα velocity offsets between 0 and 500 km s^{-1}, we predict that [C III]λ1907 would fall at 12517 –12538 Å and C III]λ1909 would fall at 12531 –to 12552 Å. Both spectral windows are free of atmospheric features, but no emission lines are apparent (Fig. 4c). The non-detection implies that each component of the [C III], C III] doublet has a flux less than 3.2×10^{-18} erg cm^{-2} s^{-1} (3σ). Given the underlying continuum flux density, this indicates the total [C III], C III] EW is below 15.6 Å, ruling out the extreme metal line emission seen in many other lensed LAEs (e.g. Christensen et al. 2012; Stark et al. 2014; Vanzella et al. 2016).

We also obtained MOSFIRE observations of A2218−C1, a triply imaged galaxy at $z \simeq 6.7$ that is among the brightest known ($H_{160} = 23.9$, 24.1, and 25.8 for images C1a, C1b, and C1c, respectively) in the reionization era. Our mask contained slits on C1.b and C1.c. The lensing configuration of the multiple images rules out any lower redshift interpretation of the SED (Kneib et al. 2004), providing independent verification that the source is at very high redshift. Unlike most of the galaxies discussed in this paper, A2218−C1 does not have powerful Lyα emission (Kneib et al. 2004; Egami et al. 2005), but its brightness should allow other UV lines to be detected if they are strong. After correcting for source magnification ($\mu = 25$ for images a and b), the absolute UV magnitude of C1 is $M_{\rm UV} = -19.4$. The *J*-band MOSFIRE spectrum we have obtained covers between 11530 and 13520 Å. Assuming the source is situated at its photometric redshift ($z = 6.65 \pm 0.1$; Egami et al. 2005), this wavelength range constrains the strength of C IV, He II, and O III] emission. We see no emission line in the spectrum of A2218−C1.b or in the fainter image A2218−C1.c. The 5σ line flux limit in regions between atmospheric OH lines (≃57 per cent of the spectrum) is 7.1×10^{-18} erg cm^{-2} s^{-1}. Given the continuum brightness of C1b, this corresponds to a rest-frame EW of 5.5 Å after applying an aperture correction of 1.33× to the line flux. While it is conceivable that one or more of the UV lines could be obscured by a sky line, the non-detection of any lines in the *J* band (and in the *z* band; Kneib et al. 2004) does suggest that A2218−C1 is not likely to be an extreme UV line emitter. Thus far, we have yet to robustly detect intense UV metal lines in a $z \gtrsim 6$ source that was not also shown to have Lyα emission, consistent with the idea that the LAEs that are currently visible at $z > 7$ are those objects with the most extreme radiation fields. *JWST* spectral observations of very bright reionization-era systems that lack Lyα should easily be able to confirm this picture.

3.5 SDSS J1414+5446

The galaxy SDSS J1414+5446 is one of the brightest ($i_{\rm AB} = 23.0$) known at $z > 5$ (McGreer et al. 2018). The source is thought to be lensed by a foreground cluster with a magnification factor in the range $5 < \mu < 25$ (McGreer et al. 2018), implying absolute UV magnitudes between $M_{\rm UV} = -21.2$ and −19.5. Extremely strong Lyα emission (EW = 260 Å rest frame) indicates a redshift of $z_{\rm Ly\alpha} = 5.426$, and the detection of NIV]λ1487 suggests a hard radiation field is likely present. Based on the absence of N V and C IV, McGreer et al. (2018) conclude that the source is not likely to be powered by an AGN.

Given the strong Lyα and NIV] emission, this object is a prime candidate for having prominent C III] emission. The new *J*-band LUCI spectrum covers 11680–13195 Å, providing coverage at the rest-frame wavelengths (1820–2038 Å) necessary to constrain the strength of C III]. For this source, we can use the systemic redshift implied by NIV] ($z_{\rm sys} = 5.424$) to calculate the wavelengths for [C III]λ1907 (12248 Å) and for C III]λ1909 (12261 Å). As shown in Fig. 4, the spectral windows contain a strong line which might affect one of the two C III] doublet component, but not both. No clear detection of [C III]λ1907 or C III]λ1909 is visible in the LUCI spectrum. We estimate a 3σ limiting flux (EW) of 1.2×10^{-17} erg cm^{-1} s^{-1} (7.3 Å) for [C III]λ1907 and 8.4×10^{-18} erg cm^{-1} s^{-1} (5.2 Å) for C III]λ1909. The absence of C III] (<12.5 Å) rules out the extreme line emission seen in many other strong LAEs at lower redshifts. While C III] EW does appear to correlate with Lyα EW (Shapley et al. 2003; Stark et al. 2014; Rigby et al. 2015; Le Fèvre et al. 2017; Maseda et al. 2017), clearly strong metal line emission is not completely ubiquitous among the most extreme EW LAEs.

3.6 Abell 383−2211

A383−2211 was first identified as a dropout by Bradley et al. (2014) in deep *HST* imaging of the cluster Abell 383. The galaxy is bright ($H_{160} = 25.2$) and magnified by $\mu = 1.5$. After correcting for this magnification, the UV absolute magnitude is found to be $M_{\rm UV} = -20.9$, similar to that of an $L^{\star}_{\rm UV}$ $z \simeq 6$ galaxy (e.g. Bouwens et al. 2015b). The broad-band SED suggests a photometric redshift of $z = 6.0^{+0.2}_{-0.3}$ (Bradley et al. 2014), but prior to this work the object lacked a spectroscopic redshift.

Our VLT/X-shooter observations of A383−2211 target Lyα along with N V, C IV, He II, O III], and C III]. At $z \simeq 6.0$, we would expect Lyα in the visible arm of X-shooter. A strong emission line is seen to peak at 8547.6 Å (Fig. 5). The asymmetry of the observed line profile and absence of other lines in the VIS and NIR arms indicates this feature is Lyα. Adopting the wavelength of the peak flux, we derive a redshift of $z_{\rm Ly\alpha} = 6.031$, nearly identical to the photometric redshift. The integrated flux of Lyα is $16.4 \pm 1.4 \times 10^{-18}$ erg

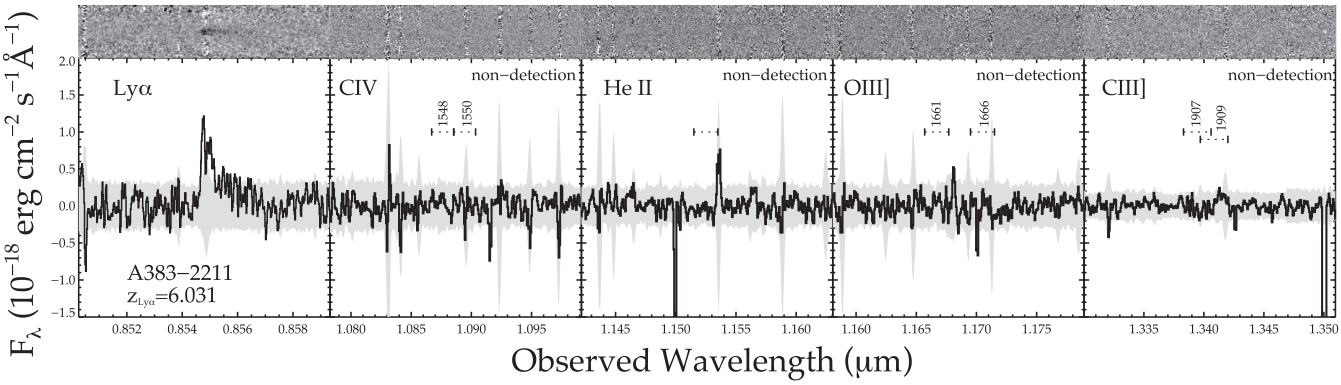

Figure 5. X-Shooter 2D spectrum (top) and 1D spectrum (bottom) of Abell 383−2211 showing the spectral region of Lyα, C IV, He II, O III], and C III], respectively, from left to right. Lyα at $z_{\rm Ly\alpha} = 6.031$ is clearly visible at 0.8547 μm. The black curve denotes the extracted 1D flux, whereas the grey region indicates 1σ noise level. The dotted black lines represent the expected spectral window where the relevant lines would fall. See Section 3.5 for details.

cm^{-2} s^{-1} corresponding to a rest-frame Lyα EW of 21.1 ± 2.8 Å. The redshift of A383−2211 is similar to that of another lensed LAE (A383−5.2) behind Abell 383 at $z = 6.027$ (Richard et al. 2011b), suggesting a likely association between the two systems. Strong C III] emission has been previously detected in the $z = 6.027$ LAE (Stark et al. 2015a); if A383−2211 has similar stellar populations and gas conditions, we might expect to see similar metal line emission in the NIR arm of the X-Shooter spectrum.

We use the Lyα redshift to predict the wavelengths of the fainter UV metal lines. Allowing for Lyα velocity offsets in the range 0–500 km s^{-1}, we predict spectral windows for N Vλ1238 (8690.0–8710.0), N Vλ1243 (8723.5–8738.1), He II (11515.3–11534.5 Å), O III]λ1661 (11657.7–11677.2 Å), O III]λ1666 (11695.2–11714.7 Å), [C III]λ1907 (13383.5–13405.9 Å), and C III]λ1909 (13397.9–13420.3 Å). For the resonant C IV doublet, we again allow redshifts between $z_{\rm sys} = 6.019$ and 6.031, implying a wavelength range of 10867.2–10885.3 Å for C IVλ1548 and 10885.3–10903.5 Å for C IVλ1550. The windows specified are mostly free of atmospheric emission features (Fig. 5), with OH lines taking up no more than 15 per cent of any given window. As can be seen from Fig. 5, no emission lines are present. The derived line flux limits are listed in Table 2. We place 3σ upper limits on the rest-frame EWs of N Vλλ1238,1243 (4.9 and 4.9 Å), C IVλλ1548,1550 (3.8 and 5.3 Å), He IIλ1640 (4.6 Å), O III]λλ1661,1666 (3.5 and 8.6 Å), [C III], and C III]λλ1907,1909 (9.6 and 12.9 Å). The absence of strong C III] suggests this object has a less extreme radiation field than the nearby galaxy A383 − 5.2, as might be expected based off of the lower Lyα EW.

4 DISCUSSION AND CONCLUSIONS

4.1 The origin of N V emission in EGSY8p7

In Section 3.1, we presented the detection of N Vλ1243 in the spectrum of EGSY8p7, a colour-selected Lyα-emitting galaxy at $z_{\rm Ly\alpha} = 8.683$ (Zitrin et al. 2015, RB16). The N V line can have its origin in either H II regions or stellar winds. The stellar wind feature is commonly seen in high-redshift galaxy spectra (e.g. Shapley et al. 2003; Jones, Stark & Ellis 2012; Steidel et al. 2016; Rigby et al. 2018). Population synthesis models including single stellar populations (e.g. Leitherer et al. 1999) and binary stars (Eldridge & Stanway 2016) both predict that the N V stellar wind feature can be prominent, particularly at very young ages. But the EW of the N Vλ1243 component in these models does not reach higher than 2.5 Å, less than the value we measure in the spectrum of EGSY8p7. The emission component of the stellar wind profile is typically observed to be very broad (>1000 km s^{-1}) reflecting the terminal velocity of the winds. While it is conceivable that broader wings are too faint to be detected in the *J*-band spectrum, this would imply a total EW that is even larger than what we report, putting the observations further at odds with the stellar wind model predictions. We thus conclude that the line observed in EGSY8p7 is most likely to be nebular in origin. Nevertheless, the N V detections that are now emerging at $z > 7$ motivate both theoretical and observational investigations of the range of N V EWs and linewidths that can produced by the winds of massive stars.

Powering nebular N V emission requires an EUV spectrum with substantial flux above 77 eV. Because the spectra of hot stars have a strong break above 54 eV, the presence of N V in EGSY8p7 likely points to either AGN activity or fast radiative shocks. The flux ratio of UV lines can help to distinguish between the two (e.g. Groves, Dopita & Sutherland 2004; Allen et al. 2008; Feltre et al. 2016). The non-detections of C IV and He II in EGSY8p7 allow us to place upper limits on the N V/C IV flux ratio (>2.6[1.6] at 3[5]σ) and N V/He II flux ratio (>3.8[2.2] at 3[5]σ), provided that both lines are not obscured by skylines. While this is not a concern for C IV (see Fig. 2), there is a strong skyline that covers 19 per cent of the predicted He II spectral window. If the N Vλ1243 feature has the same redshift as He II, the latter would indeed be located very close to this skyline. We thus consider the N V/He II limit to be less robust than N V/C IV. The constraints on the line ratios in EGSY8p7 are broadly consistent with those in COSY, another LAE from the RB16 sample with N V emission (Laporte et al. 2017) and several luminous LAEs at $z \sim 2$–3 (Sobral et al. 2018). Both sources have N V/C IV flux ratios slightly greater than unity, in marginal tension with many AGN and shock models with standard abundance ratios (e.g. Groves et al. 2004; Allen et al. 2008; Feltre et al. 2016; Laporte et al. 2017). Nevertheless, there are examples of AGNs with N V/C IV$\simeq$ 1 in high-redshift samples from the Sloan Digital Sky Survey (Alexandroff et al. 2013). As noted in Laporte et al. (2017), additional physics or resonant scattering of C IV photons might ultimately be required to explain the N V/C IV flux ratios that are emerging at $z > 7$. While distinguishing between shocks and AGN is clearly difficult with only an N V detection, the launch of *JWST* will provide a wealth of UV and optical spectral constraints on EGSY8p7, clarifying the origin of the intense line emission.

With the N v detection in the Zitrin et al. (2015) $z = 8.68$ galaxy, three of the 13 Lyα-emitting galaxies known at $z > 7$ have been shown to have N v emission (e.g.Tilvi et al. 2016; Laporte et al. 2017), and two other have recently been detected in LAEs at $z = 6.9$ (Hu et al. 2017) and $z = 6.6$ (Sobral et al. 2017a). The $z > 7$ systems with N v emission are among the most luminous (1.3–2.5× greater than $L^{\star}_{UV}$) and massive galaxies known at $z > 7$. It is perhaps not surprising that signs of supermassive black hole growth would be detected in such massive early systems. At lower redshifts AGNs are present in LAEs samples, but the AGN fractions are generally less than 5–10 per cent (e.g. Ouchi et al. 2008; Zheng et al. 2010; Sobral et al. 2017b; Shibuya et al. 2017). But recent work indicates that this fraction increases in the more luminous LAEs (Sobral et al. 2018). While further work is certainly needed to isolate the powering mechanism of the N v detections, these early studies appear to indicate that the known LAEs at $z > 7$ contain a large fraction of sources with hard ionizing spectra, as might be expected if the extreme radiation field enhances the visibility of Lyα through the partially neutral IGM.

4.2 The frequency of C III] and C IV emission at $z > 7$

The UV metal line emission observed in $z > 6$ galaxies (Stark et al. 2015a,b, 2017; Tilvi et al. 2016; Mainali et al. 2017; Schmidt et al. 2017; Laporte et al. 2017; Matthee et al. 2017) is a marked departure from the weak line emission typically found at lower redshift (e.g. Shapley et al. 2003; Rigby et al. 2015; Du et al. 2017, 2018), motivating theoretical investigations into the factors regulating UV line spectra (Jaskot & Ravindranath 2016; Gutkin et al. 2016; Nakajima et al. 2017; Volonteri et al. 2017; Byler et al. 2018) and observational efforts to identify intense UV line emitters locally and at $z \simeq 1$–3 (Stark et al. 2014; Rigby et al. 2015; Du et al. 2017; Senchyna et al. 2017; Maseda et al. 2017; Le Fèvre et al. 2017; Amorín et al. 2017). With a larger sample of $z > 5$ galaxies with UV metal line constraints (see Table 2), we can now begin to investigate to what extent the extreme UV line emitters are representative among reionization-era sources.

While C IV emission has been absent in the sources with likely N v detections, the nebular line has been detected in two star-forming galaxies at $z > 6$ (Stark et al. 2015b; Mainali et al. 2017; Schmidt et al. 2017). In contrast to the galaxies with N v emission, the C IV emitters are among the lowest luminosity galaxies with detectable Lyα emission in the reionization era. Both are gravitationally lensed with absolute UV magnitudes ($M_{UV} = -20.1, -19.3$) that are 2.8–5.8× lower than the median luminosity of the three $z > 7$ sources with reported N v emission. The presence of C IV requires a significant supply of 48 eV photons capable of triply ionizing carbon. Local UV spectral data bases (e.g. Berg et al. 2016; Senchyna et al. 2017) show that nebular C IV emission becomes commonplace in actively star-forming galaxies with gas-phase metallicities below 12+log O/H $\simeq$ 8.0, a consequence of the rapid transition in the hardness of the EUV spectrum of massive stars below this metallicity threshold (Senchyna et al. 2017). The sharp increase in hard photons can be explained in part by less dense stellar winds (which allow more of the EUV flux to escape the stellar atmospheres) and more efficient evolutionary pathways toward the creation of hot stripped stars at low metallicity (e.g. Senchyna et al. 2017). The detection of strong nebular C IV emission may thus be able to provide a valuable signpost of low-metallicity stellar populations. In Fig. 6, we show the relationship between M_{UV} and C IV EW for galaxies at $z \gtrsim 5$, updating a plot originally presented in Shibuya et al. (2017)

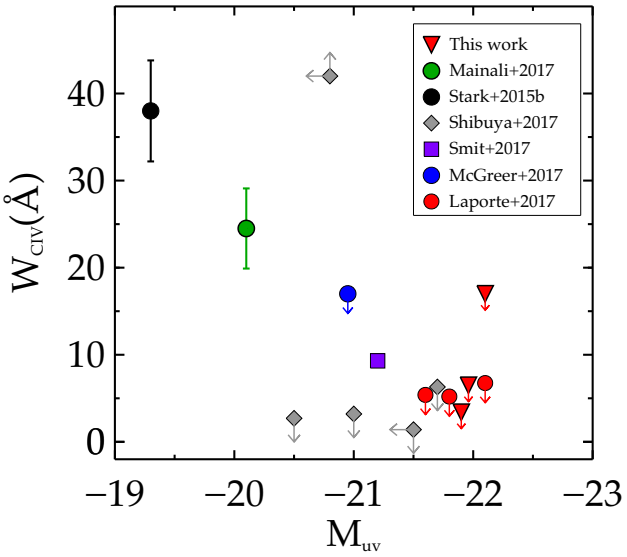

Figure 6. Plot of rest-frame C IV EW ($W_{C IV}$) as a function of M_{UV}. The red triangles are $z \sim 7$–9 sources from this paper. The other symbols are compilation from the literature: red circle (Laporte et al. 2017); grey diamond (Shibuya et al. 2017); violet square (Smit et al. 2017); blue circle (McGreer et al. 2018); green circle (Mainali et al. 2017); and black circle (Stark et al. 2015b). These existing studies reveal C IV emission only in the lowest luminosity galaxies, consistent with trends found locally and at lower redshifts.

with the new upper limits presented in this paper. The presence of C IV is limited to the lowest luminosity systems, as might be expected if a luminosity–metallicity relationship is present at these early times. In this context, the absence of strong C IV emission in the luminous RB16 sources may indicate that metallicity of massive stars in these systems has already been polluted above the threshold necessary for powering a hard EUV spectrum. *JWST* will soon begin to provide constraints on the rest-optical lines in these and other reionization-era galaxies, making it possible to investigate the relationship between high ionization UV lines and metallicity in more detail.

Much of the attention on metal lines has focused on the [C III], C III] doublet, as it is often the strongest line in the UV other than Lyα. Intense [C III], C III] emission (EW=22Å) has been detected in EGS-zs8-1, the $z = 7.73$ LAE from the RB16 sample (Oesch et al. 2015; Stark et al. 2017). Similarly strong C III] (EW = 22.5 Å) is present in A383−5.2 (Stark et al. 2015a), a gravitationally lensed $z = 6.03$ galaxy with Lyα (Richard et al. 2011b). In this paper, we present upper limits on the strength of C III] in five sources at $z > 5.4$. When taken together with robust limits from the literature (see Table 3), we find that the fraction of galaxies at $z > 5.4$ with C III] EW>20 Å is 0.14 ± 0.10. While such strong C III] emission is clearly not ubiquitous among reionization-era galaxies, it is even less common among systems at lower redshifts. In a study of 2543 galaxies at $2 < z < 3.8$, Le Fèvre et al. (2017) find only 31 sources with C III] EW in excess of 20 Å, implying a fraction of just 1.2 per cent. Similarly low fractions are found in other studies of galaxies at $z \simeq 0$–3 (Rigby et al. 2015; Du et al. 2017; Senchyna et al. 2017). These preliminary indications of evolution in the fraction of extreme EW C III] emitters (Fig. 7) could be interpreted as a byproduct of the changing demographics of star-forming galaxies; as larger sSFR and more intense optical line emission become more common at early times, strong C III] emission should simi-

Table 3. Compilation of spectroscopically confirmed galaxies from the literature with robust C III] EW ($W_{CIII],0}$) constraints. We limit the compilation to those systems with known redshifts and spectroscopic constraints that are deep enough to rule out or confirm extreme (i.e. >20 Å) EW [C III],C III] emission. References: [1] Stark et al. (2017); [2] Watson et al. (2015);[3] Laporte et al. (2017); [4] Mainali et al. (2017); [5] Schmidt et al. (2017); [6] Stark et al. (2015a); [7] Stark et al. (2015b); and [8] Ding et al. (2017).

Object	z_{spec}	Line	λ_{rest} (Å)	Line flux (10^{-18} erg cm^{-2} s^{-1})	$W_{CIII],0}$ (Å)	M_{UV} (AB)	References
EGS-zs8-1	7.730	[C III]	1906.68	4.5 ± 0.5	12 ± 2	−22.1	[1]
	...	C III]	1908.73	3.6 ± 0.5	10 ± 1	...	[1]
A1689-zD1	7.5	[C III]	1909	<2	<4	−20.1	[2]
EGS-zs8-2	7.477	[C III]	1906.68	<2.3	<7.1	−21.9	[1]
	...	C III]	1908.73	<2.3	<7.1	...	[1]
COSY	7.149	[C III]	1906.68	<0.92	<3.6	−21.8	[3]
	...	C III]	1908.73	<0.83	<3.2	...	[3]
COSz1	6.854	[C III]	1906.68	<1.18	<3.7	−21.6	[3]
	...	C III]	1908.73	1.33 ± 0.3	4.1 ± 0.9	...	[3]
COSz2	6.816	[C III]	1906.68	<1.57	<5.5	−22.1	[3]
	...	C III]	1908.73	<1.57	<5.5	...	[3]
RXCJ2248.7-4431	6.110	[C III]	1909	<3.6	<7.9	−20.1	[4],[5]
A383−5.2	6.027	[C III]^a	1906.68	5.2 ± 1.6	13.1 ± 3.9	−19.3	[6]
	...	C III]	1908.73	3.7 ± 1.1	9.4 ± 2.8	...	[6]
A1703−23	5.828	[C III]	1906.68	<1.5	<1.1	−21.7	[7]
	...	C III]	1908.73	<3.4	<2.6	...	[7]
Ding-3	5.75	[C III]	1909	<3.3	<15.1	−20.9	[8]
Ding-1	5.70	[C III]	1909	<5.4	<6.6	−22.2	[8]
Ding-2	5.69	[C III]	1909	<3.4	<4.5	−22.2	[8]

Note. ^{a}Line flux for [C III]λ1907 is calculated assuming [C III]λ1907/C III]λ1909=1.4.

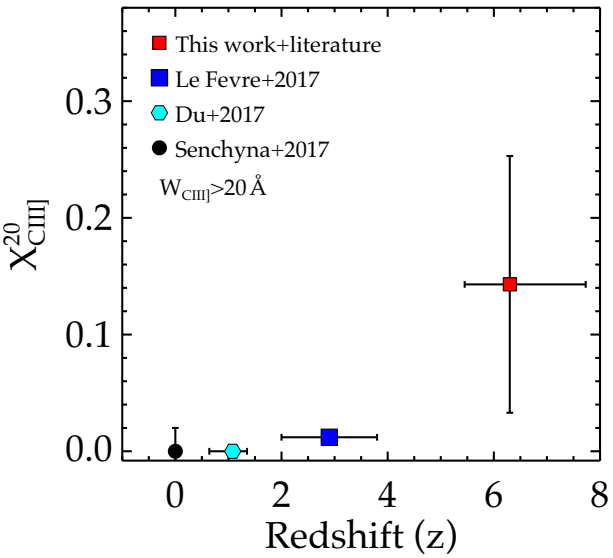

Figure 7. Fraction of strong C III] emitters ($W_{CIII]} > 20$ Å) as a function of redshift. The fraction at $z \sim 0$, 1, and 3 are computed using data from Senchyna et al. (2017), Du et al. (2017), and Le Fèvre et al. (2017), respectively. The fraction at $z \sim 5.5$–9 is calculated using data in Tables 2 and 3. We note that the parent sample at $z \sim 5.5$–9 is derived from spectroscopically confirmed sources with constraints on C III] emission.

larly become more typical (e.g. Senchyna et al. 2017; Maseda et al. 2017). Others have put forth an alternative explanation, arguing that sources with C III] EW>20 Å likely have AGN activity (Nakajima et al. 2017); in this picture, the increased incidence of extreme C III] emitters may reflect the changing nature of LAEs at $z \simeq 7$–8. One other important factor that could possibly govern the strength of carbon lines is the relative C/O abundance (Stark et al. 2014; Berg et al. 2016; Nakajima et al. 2017; Le Fèvre et al. 2017; Berg et al. 2018). These papers show that C/O decreases at lower O/H over $0.1 \leq Z/Z_{\odot} \leq 1.0$. If C/O is very low at $z > 6$, it could cause the lines to be weaker than expected. However, measurements of C/O at $z > 6$ are not yet possible with current facilities. Future observations that simultaneously detect C III], C IV, and O III] at $z > 6$ will shed light on the role of C/O abundance in shaping the strength of carbon lines in these early galaxies.

While our knowledge of the UV line statistics is undoubtedly still in its infancy, the presence of intense line emission is beginning to refine our understanding of the nature of the LAE population in the reionization era. Prominent emission lines (N V, C IV, or C III]) have now been reported in five of the 13 LAEs known at $z > 7$. Galaxies with similar Lyα EW at lower redshifts (e.g. Shapley et al. 2003; Jones et al. 2012; Du et al. 2017; Le Fèvre et al. 2017) very rarely exhibit such extreme UV line emission. These results continue to suggest that the radiation field is playing an important role in making these systems visible in Lyα emission in an epoch where most Lyα photons are strongly attenuated by the IGM. Attempts to map the evolving Lyα EW distribution to a neutral hydrogen fraction must ultimately take into account these variations in the radiation field. The launch of *JWST* will soon provide an opportunity to extend rest-UV studies to larger samples, increasing our understanding of the factors regulating the escape of Lyα in the reionization era. While many of the spectroscopic studies will focus on the strong rest-optical lines, the UV should not be neglected as the presence of various high ionization features (N V, He II, and C IV) provides the most direct path toward detecting extreme sources, whether they be AGN or very low metallicity stellar populations.

ACKNOWLEDGEMENTS

We thank referee for the useful suggestions and comments. We are very grateful to Anna Feltre for enlightening conversations.

DPS acknowledges support from the National Science Foundation through the grant AST-1410155. RSE and NL acknowledge support from the European Research Council through an Advanced Grant FP7/669253. JR acknowledges support from the European Research Council through a Starting grant FP7/336736. This work was partially supported by a NASA Keck PI Data Award, administered by the NASA Exoplanet Science Institute. Data presented herein were obtained at the W. M. Keck Observatory from telescope time allocated to the National Aeronautics and Space Administration through the agency's scientific partnership with the California Institute of Technology and the University of California. The Observatory was made possible by the generous financial support of the W. M. Keck Foundation. The authors acknowledge the very significant cultural role that the summit of Mauna Kea has always had within the indigenous Hawaiian community. We are most fortunate to have the opportunity to conduct observations from this mountain. Also based on observations made with ESO Telescopes at the La Silla Paranal Observatory under programme ID 092.A-0630(A). The LBT is an international collaboration among institutions in the United States, Italy, and Germany. LBT Corporation partners are: The University of Arizona on behalf of the Arizona university system; Istituto Nazionale di Astrofisica, Italy; LBT Beteiligungsgesellschaft, Germany, representing the Max-Planck Society, the Astrophysical Institute Potsdam, and Heidelberg University; The Ohio State University, and The Research Corporation, on behalf of The University of Notre Dame, University of Minnesota and University of Virginia.

REFERENCES

Alexandroff R. et al., 2013, MNRAS, 435, 3306
Allen M. G., Groves B. A., Dopita M. A., Sutherland R. S., Kewley L. J., 2008, ApJS, 178, 20
Amorín R. et al., 2017, Nat. Astron., 1, 0052
Atek H. et al., 2015, ApJ, 814, 69
Bañados E. et al., 2018, Nature, 553, 473
Bayliss M. B., Rigby J. R., Sharon K., Wuyts E., Florian M., Gladders M. D., Johnson T., Oguri M., 2014, ApJ, 790, 144
Berg D. A., Skillman E. D., Henry R. B. C., Erb D. K., Carigi L., 2016, ApJ, 827, 126
Berg D. A., Erb D. K., Auger M. W., Pettini M., Brammer G. B., 2018, ApJ, 859, 164
Bian F. et al., 2010, ApJ, 725, 1877
Bian F. et al., 2015, ApJ, 806, 108
Bickel W., 1969, J. Quant. Spec. Radiat. Transf., 9, 1145
Bosman S. E. I., Becker G. D., 2015, MNRAS, 452, 1105
Bouwens R. J., Illingworth G. D., Oesch P. A., Caruana J., Holwerda B., Smit R., Wilkins S., 2015a, ApJ, 811, 140
Bouwens R. J. et al., 2015b, ApJ, 803, 34
Bradley L. D. et al., 2012, ApJ, 747, 3
Bradley L. D. et al., 2014, ApJ, 792, 76
Byler N., Dalcanton J., Conroy C., Johnson B., Levesque E., Berg D., 2018, preprint (arXiv:1803.04425)
Caruana J., Bunker A. J., Wilkins S. M., Stanway E. R., Lorenzoni S., Jarvis M. J., Ebert H., 2014, MNRAS, 443, 2831
Christensen L. et al., 2012, MNRAS, 427, 1953
Dijkstra M., Wyithe S., Haiman Z., Mesinger A., Pentericci L., 2014, MNRAS, 440, 3309
Ding J. et al., 2017, ApJ, 838, L22
Dors O. L., Cardaci M. V., Hägele G. F., Krabbe Â. C., 2014, MNRAS, 443, 1291
Du X., Shapley A. E., Martin C. L., Coil A. L., 2017, ApJ, 838, 63
Du X. et al., 2018, ApJ, 860, 75
Ebbels T. M. D., Le Borgne J.-F., Pello R., Ellis R. S., Kneib J.-P., Smail I., Sanahuja B., 1996, MNRAS, 281, L75
Egami E. et al., 2005, ApJ, 618, L5
Eldridge J. J., Stanway E. R., 2016, MNRAS, 462, 3302
Elíasdóttir Á. et al., 2007, preprint (arXiv:0710.5636)
Ellis R., Santos M. R., Kneib J.-P., Kuijken K., 2001, ApJ, 560, L119
Erb D. K. et al., 2014, ApJ, 795, 33
Feltre A., Charlot S., Gutkin J., 2016, MNRAS, 456, 3354
Finkelstein S. L. et al., 2015, ApJ, 810, 71
Fontana A. et al., 2010, ApJ, 725, L205
Furusawa H. et al., 2016, ApJ, 822, 46
Greig B., Mesinger A., Haiman Z., Simcoe R. A., 2017, MNRAS, 466, 4239
Groves B. A., Dopita M. A., Sutherland R. S., 2004, ApJS, 153, 9
Gutkin J., Charlot S., Bruzual G., 2016, MNRAS, 462, 1757
Hu E. M., Cowie L. L., Barger A. J., Capak P., Kakazu Y., Trouille L., 2010, ApJ, 725, 394
Hu W. et al., 2017, ApJ, 845, L16
Ishigaki M., Kawamata R., Ouchi M., Oguri M., Shimasaku K., Ono Y., 2018, ApJ, 854, 73
James B. L. et al., 2014, MNRAS, 440, 1794
Jaskot A. E., Ravindranath S., 2016, ApJ, 833, 136
Jones T., Stark D. P., Ellis R. S., 2012, ApJ, 751, 51
Kashikawa N. et al., 2006, ApJ, 648, 7
Kneib J.-P., Ellis R. S., Smail I., Couch W. J., Sharples R. M., 1996, ApJ, 471, 643
Kneib J.-P., Ellis R. S., Santos M. R., Richard J., 2004, ApJ, 607, 697
Konno A. et al., 2018, PASJ, 70, S16
Laporte N., Nakajima K., Ellis R. S., Zitrin A., Stark D. P., Mainali R., Roberts-Borsani G. W., 2017, ApJ, 851, 40
Le Fèvre O. et al., 2017, A&A, preprint (arXiv:1710.10715)
Leitherer C. et al., 1999, ApJS, 123, 3
Livermore R. C., Finkelstein S. L., Lotz J. M., 2017, ApJ, 835, 113
Mainali R., Kollmeier J. A., Stark D. P., Simcoe R. A., Walth G., Newman A. B., Miller D. R., 2017, ApJ, 836, L14
Malhotra S., Rhoads J. E., 2004, ApJ, 617, L5
Maseda M. V. et al., 2017, A&A, 608, A4
Mason C. A., Treu T., Dijkstra M., Mesinger A., Trenti M., Pentericci L., de Barros S., Vanzella E., 2017, ApJ, 856, 2
Mason C. A. et al., 2018, ApJ, 857, L11
Matthee J., Sobral D., Darvish B., Santos S., Mobasher B., Paulino-Afonso A., Röttgering H., Alegre L., 2017, MNRAS, 472, 772
McGreer I. D., Mesinger A., D'Odorico V., 2015, MNRAS, 447, 499
McGreer I. D. et al., 2018, MNRAS, preprint (arXiv:1706.09428)
McLean I. S. et al., 2012, Proc. SPIE, 8446, 84460J
McLure R. J. et al., 2013, MNRAS, 432, 2696
Mesinger A., Aykutalp A., Vanzella E., Pentericci L., Ferrara A., Dijkstra M., 2015, MNRAS, 446, 566
Mortlock D. J. et al., 2011, Nature, 474, 616
Nakajima K. et al., 2017, A&A, 612, A94
Oesch P. A. et al., 2015, ApJ, 804, L30
Oke J. B., Gunn J. E., 1983, ApJ, 266, 713
Ono Y. et al., 2012, ApJ, 744, 83
Ota K. et al., 2017, ApJ, 844, 85
Ouchi M. et al., 2008, ApJS, 176, 301
Ouchi M. et al., 2010, ApJ, 723, 869
Pentericci L. et al., 2014, ApJ, 793, 113
Pentericci L. et al., 2016, ApJ, 829, L11
Planck Collaboration I, 2016, A&A, 594, A1
Richard J. et al., 2007, ApJ, 662, 781
Richard J., Jones T., Ellis R., Stark D. P., Livermore R., Swinbank M., 2011a, MNRAS, 413, 643
Richard J., Kneib J.-P., Ebeling H., Stark D. P., Egami E., Fiedler A. K., 2011b, MNRAS, 414, L31
Rigby J. R., Bayliss M. B., Gladders M. D., Sharon K., Wuyts E., Dahle H., Johnson T., Peña-Guerrero M., 2015, ApJ, 814, L6
Rigby J. R. et al., 2018, ApJ, 853, 87
Roberts-Borsani G. W. et al., 2016, ApJ, 823, 143 (RB16)
Robertson B. E., Ellis R. S., Furlanetto S. R., Dunlop J. S., 2015, ApJ, 802, L19

Schenker M. A., Stark D. P., Ellis R. S., Robertson B. E., Dunlop J. S., McLure R. J., Kneib J.-P., Richard J., 2012, ApJ, 744, 179
Schenker M. A., Ellis R. S., Konidaris N. P., Stark D. P., 2014, ApJ, 795, 20
Schmidt K. B. et al., 2016, ApJ, 818, 38
Schmidt K. B. et al., 2017, ApJ, 839, 17
Senchyna P. et al., 2017, MNRAS, 472, 2608
Shapley A. E., Steidel C. C., Pettini M., Adelberger K. L., 2003, ApJ, 588, 65
Shibuya T. et al., 2017, PASJ, 70, S15
Smit R., Swinbank A. M., Massey R., Richard J., Smail I., Kneib J.-P., 2017, MNRAS, 467, 3306
Sobral D. et al., 2017a, MNRAS, preprint (arXiv:1710.08422)
Sobral D., Santos S., Matthee J., Paulino-Afonso A., Ribeiro B., Calhau J., Khostovan A. A., 2017b, MNRAS, 476, 4725
Sobral D. et al., 2018, MNRAS, 477, 2817
Stanway E. R., Eldridge J. J., Becker G. D., 2016, MNRAS, 456, 485
Stark D. P., 2016, ARA&A, 54, 761
Stark D. P., Ellis R. S., Chiu K., Ouchi M., Bunker A., 2010, MNRAS, 408, 1628
Stark D. P. et al., 2014, MNRAS, 445, 3200
Stark D. P. et al., 2015a, MNRAS, 450, 1846
Stark D. P. et al., 2015b, MNRAS, 454, 1393
Stark D. P. et al., 2017, MNRAS, 464, 469
Steidel C. C., Strom A. L., Pettini M., Rudie G. C., Reddy N. A., Trainor R. F., 2016, ApJ, 826, 159
Tilvi V. et al., 2014, ApJ, 794, 5
Tilvi V. et al., 2016, ApJ, 827, L14
Torres-Peimbert S., Pena M., 1984, RMxAA, 9, 107
Vanzella E. et al., 2016, ApJ, 821, L27
Vanzella E. et al., 2017, ApJ, 842, 47
Vernet J. et al., 2011, A&A, 536, A105
Volonteri M., Reines A., Atek H., Stark D. P., Trebitsch M., 2017, ApJ, 849,155
Watson D., Christensen L., Knudsen K. K., Richard J., Gallazzi A., Michałowski M. J., 2015, Nature, 519, 327
Zheng Z. Y., Wang J. X., Finkelstein S. L., Malhotra S., Rhoads J. E., Finkelstein K. D., 2010, ApJ, 718, 52
Zitrin A. et al., 2015, ApJ, 810, L12

This paper has been typeset from a TEX/LATEX file prepared by the author.